Weak-antilocalization signatures in the magnetotransport properties of individual electrodeposited Bi Nanowires

N. Marcano, S. Sangiao, M. Plaza, L. Pérez, A. Fernández Pacheco, R. Córdoba, M. C. Sánchez, L. Morellón , M. R. Ibarra, and J. M. De Teresa

Citation: Applied Physics Letters **96**, 082110 (2010); doi: 10.1063/1.3328101
View online: http://dx.doi.org/10.1063/1.3328101
View Table of Contents: http://scitation.aip.org/content/aip/journal/apl/96/8?ver=pdfcov
Published by the AIP Publishing

Weak-antilocalization signatures in the magnetotransport properties of individual electrodeposited Bi Nanowires

N. Marcano,[1,2,a] S. Sangiao,[1,2,3] M. Plaza,[4] L. Pérez,[4] A. Fernández Pacheco,[1,2,3] R. Córdoba,[2,3] M. C. Sánchez,[4] L. Morellón,[1,2,3] M. R. Ibarra,[1,2,3] and J. M. De Teresa[1,2]
[1]*Instituto de Ciencia de Materiales de Aragón, Universidad de Zaragoza-CSIC, Zaragoza 50009, Spain*
[2]*Departamento de Física de la Materia Condensada, Universidad de Zaragoza, Zaragoza 50009, Spain*
[3]*Instituto de Nanociencia de Aragón, Universidad de Zaragoza, Zaragoza 50009, Spain*
[4]*Departamento de Física de Materiales, Universidad Complutense de Madrid, Madrid 28040, Spain*

(Received 22 December 2009; accepted 30 January 2010; published online 24 February 2010)

We study the electrical resistivity of individual Bi nanowires of diameter 100 nm fabricated by electrodeposition using a four-probe method in the temperature range 5–300 K with magnetic fields up to 90 kOe. Low-resistance Ohmic contacts to individual Bi nanowires are achieved using a focused ion beam to deposit W-based nanocontacts. Magnetoresistance measurements show evidence for weak antilocalization at temperatures below 10 K, with a phase-breaking length of 100 nm. © *2010 American Institute of Physics*. [doi:10.1063/1.3328101]

During the last years, there has been a great interest in Bi nanowires (NWs) since they provide an attractive scenario for fundamental investigation of both classical and quantum finite-size effects, due to the unusual electronic structure of Bi. They are of special interest for thermoelectric applications due to the unique properties of bulk Bi, such as its small electron effective mass, the high anisotropy of its Fermi surface and the low thermal conductivity.[1] In particular, the small Bi electron effective mass ($\sim 0.001\ m_e$) has motivated an active investigation of quasi-one-dimensional (1D) phenomena such as the wire-boundary scattering effect and quantum confinement effects on the electronic transport properties of quasi 1D-systems.[2,3]

Localization effects caused by quantum interference effects in disordered systems with reduced dimensionality have been studied over the past two decades.[4] In the case of systems with large spin-orbit interaction, such as Bi, they are referred to as weak antilocalization (WAL) effects and manifest as a positive correction to the conductance of the system.[5–7] In a system with a diffusion constant D, the relevant scale for coherence in phase is $L_\varphi=(D\tau_\varphi)^{1/2}$ (τ_φ is the phase-breaking time of the electron wave function) which determines the effective dimensionality of a system with respect to WAL effects. Thus, for a wire with a small diameter (W) so that $L_\varphi > W$, the localization behavior should be regarded as 1D. In the case of Bi, the signature from WAL effects can be overshadowed by the contribution coming from the classical or ordinary magnetoresistance (MR) caused by the curving of the electron trajectory by the magnetic field (Lorentz force). In particular, Bi NW arrays show ordinary MR values of several 100 s at 50 kOe at low temperature[8] which is typically two to three orders of magnitude larger than the contribution due to WAL.[9] This fact limited the observation of signatures of localization effects to very low temperatures (<4 K) and low magnetic fields which did not allow a quantitative analysis of localization effects. However, WAL effects can be enhanced with the reduction of dimensionality since the classical MR is expected to drop significantly. NWs represent an excellent playground for the investigation of 1D WAL effects.

To date, however, most of the reported studies on Bi-NWs focused on electronic transport properties in polycrystalline or single-crystal Bi arrays of NW using two-probe technique. The main reason for the lack of four-probe measurements on individual NW is the difficulty in making good electrical Ohmic contacts due to a native 10 nm thick Bi oxide coating that forms on the surface of the NWs.[10] Over last years, some research groups succeeded[10,11] although their studies focused on absolute resistivity without further fundamental transport properties such as MR. Recently, Shim *et al.*[12] carried out magnetotransport properties of an individual single-crystalline (its axis oriented along the trigonal direction [001]) 400-nm-diameter Bi NW. In that case, however, the dimension of the NW was too large and the contribution of the classical MR was too high (several thousands at low temperatures) to allow the WAL effects to be observed.

In this letter, we present the magnetotransport properties of individual single crystalline Bi NWs of 100 nm-width (smaller than the mean free path).

Bismuth NWs with an average diameter of 100 nm and 4 μm in length were fabricated by electrodeposition as described elsewhere.[13] Figure 1(a) shows the transmission electron microscopy image of an individual NW revealing that they are cylindrical in shape. X-ray diffraction and high resolution transmission electron microscopy (HRTEM) revealed a rhombohedral structure, the same as that of bulk Bi. The electron diffraction pattern obtained in the direction perpendicular to the long axis of the NW was indexed to the hexagonal lattice of Bi [Fig. 1(b)]. Figure 1(c) shows the select area electron diffraction (SAED) patterns identifying the family of planes (012), (110), and (122). An exhaustive study carried out in different zones of the NW by HRTEM and SAED confirms the single crystallinity and orientation of the Bi NWs which grow along the direction [012]. No extensive defects such as grain boundaries have been observed over the length of the wire, which confirms the monocrystalline structure. A very thin amorphous oxide shell (5 nm) has been observed.

[a]Author to whom correspondence should be addressed. Electronic mail: marcanon@unizar.es.

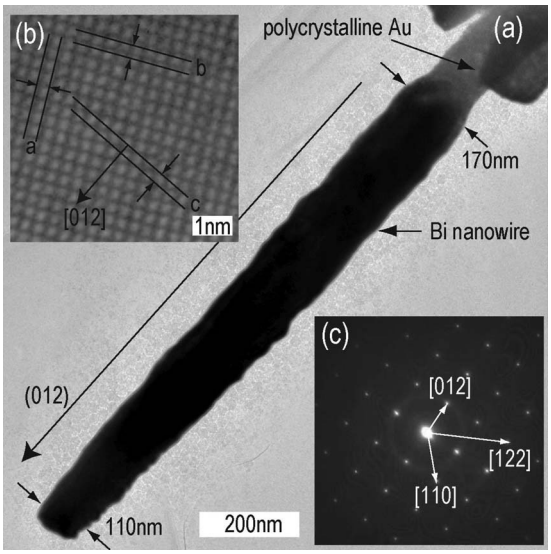

FIG. 1. (a) TEM image of 100 nm Bi NW after removing the supporting polycarbonate membrane. (b) The electron diffraction pattern taken from one of the grains. Along the NW, the diffraction patterns of different zones of NW indicate same orientation. (c) SAED pattern with the family of planes (012), (110), and (122).

For electrical measurements on a single NW, a drop of NW-containing solution is deposited onto a thermally oxidized silicon wafer where Al microelectrodes have been patterned by means of optical lithography. A relatively long NW was located by means of scanning electron microscopy (SEM) and nanoelectrodes were patterned on the NW connecting it to the Al-microelectrodes by a tungsten (W)-based nanodeposit grown by focused-ion-beam-induced-deposition (FIBID). This kind of deposit favors low electrical resistance as required in some applications.[14] SEM images of a 100 nm Bi-NW prepared using this technique are shown in Figs. 2(a) and 2(b). The resistivity ρ measured *in situ* was found to be 6×10^{-4} Ω cm, which is five times higher than the ρ of bulk Bi, 1.2×10^{-4} Ω cm. Such an increase can be explained by an ordinary size effect.[15] No modification of the resistance was observed when the NW comes into contact with ambient atmosphere, which indicates the absence of oxidation or degradation effects after exposure to ambient conditions. Magnetotransport properties have been carried out in a commercial physical properties measurement system from Quantum

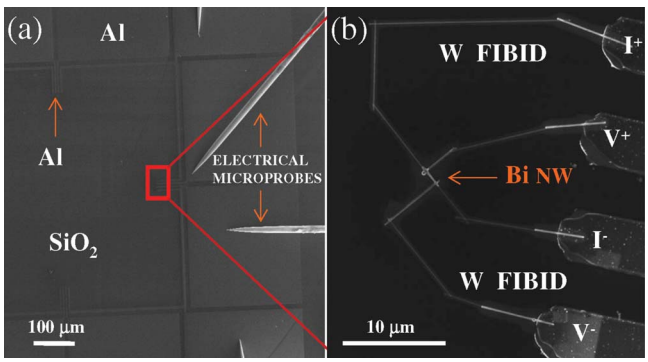

FIG. 2. (Color online) (a) SEM image of the experimental configuration for the four-probe electrical measurements. The four microprobes are contacted to Al micrometric pads patterned by optical lithography in order to perform the *in situ* measurements. The red rectangle shows the zone where the selected Bi NW is located. (b) SEM image at a higher magnification of the region where the NW is contacted with the Al micropads via the four FIBID W-nanodeposits.

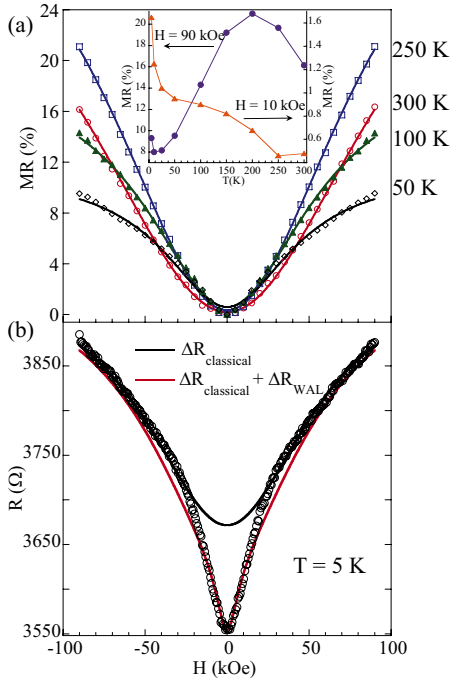

FIG. 3. (Color online) (a) MR (%) as a function of field at selected temperatures in the 50 to 300 K range for the sake of clarity. Solid lines represent fits to multiband model. Inset displays the temperature dependence of the MR (%) at 10 and 90 kOe. The solid lines are guides to the eye. (b) MR as a function of field at 5 K. The solid lines in black and red represent the classical contribution and the classical+WAL correction to the resistance according to Eq. (1), respectively.

Design in the temperature range from 300 K down to 5 K with a low-frequency current of 100 nA. The magnetic field is applied perpendicular to the substrate plane. Measurements of the NW resistance by four-probes are found to be ohmic at 5 and 300 K, corresponding to ρ of 1.83×10^{-3} and 6×10^{-4} Ω cm, respectively. This fact indicates that the observed 5 nm-thick Bi oxide shell has been either partly removed during the contact fabrication using the ion-beam or, if still present, is not thick enough to disrupt the electrical transport.

We have studied the MR $(H,\ \mathrm{T})\ (\%)=100\times\{[R(H,\mathrm{T})-R(0,\mathrm{T})]/R(0,\mathrm{T})\}$ down to low temperatures in order to highlight the contribution from WAL. Figure 3 shows the magnetic field dependence of the MR. The values of MR at 90 kOe (~16% at 300 K and ~10% at 5 K) are significantly lower than those reported by Shim *et al.*[12] We became aware that two temperature regimes can be distinguished as follows: (i) The high temperature regime ($T>10$ K), where the field dependence of MR is essentially quadratic (Lorentz) and shows no sign of saturation at high field and (ii) the low temperature regime ($T\leq10$ K), where MR shows a diplike shape near $H=0$, which is significantly enhanced as T decreases down to 5 K. This behavior is a signature of WAL.[4] In this low-temperature regime, the classical MR tends to dominate the magnetotransport for $H>12$ kOe. It is worth noting the relative high value of H up to which WAL signatures are visible. Inset of Fig. 3(a) shows that at 90 kOe the MR increases with decreasing temperature reaching its peak value at T~200 K. At low fields ($H=10$ kOe) however, MR increases sharply for $T\leq10$ K which, again, is a signature of localization effects.[6]

We have used a standard multiband model[16] to fit the experimental MR data at $T>10$ K. Each band has two pa-

rameters, resistivity ρ_i and Hall coefficient $R_i=1/q_i n_i$, where $q_i=\pm e$ is the charge of the carrier. A two-band model, with a bulk electron and a bulk hole band, accounts for the field dependence of the MR in the temperature range 100 K$<$T$<$300 K. For 10 K$<$T$<$100 K, a third electron band is required. Such a minority electron band accounts for the surface states in Bi, which are highly metallic in contrast to the semimetallic nature of bulk Bi.[17] Both theoretical and experimental works[17] have shown the important role of these states in the transport properties of Bi systems when dimensions downsizes to nanometer scale as occurs in Bi NWs.[18] It should be noted that the contribution of the surface states to the MR indicates that such states have not been quenched by the possible Bi oxide shell present in the NWs. The solid lines in Fig. 3(a) are calculated from our two- and three-band analysis. The surface carriers become important below 50 K, although bulk electrons are dominant. The ratio of bulk electrons to surface carrier density is 10 for these 100 nm-width NWs at low temperatures.

For T$\leq$10 K the three-band model only reproduces the experimental MR curves for $H\geq 12$ kOe, i.e., when classical MR dominates the magnetotransport. This is shown in Fig. 3(b) for T=5 K. The dip in the MR for $H<12$ kOe requires being analyzed in accordance with WAL theory. The correction to the resistance due to WAL in 1D systems in the strong spin-orbit limit is predicted to take the form:[19,20]

$$\frac{\Delta R_{\mathrm{WAL}}}{R_0}=\frac{1}{\sqrt{2}}\frac{e^2}{\pi\hbar}\frac{R_{\square}L_{\varphi}}{W}A_i(x)\left\{\frac{d}{dx}[A_i(x)]\right\}^{-1}, \qquad (1)$$

where $A_i(x)$ denotes the Airy function, $R_{\square}$ is the resistance per square which in the present case takes the form $R_{\square}=\rho/W$ and $x=2(L_{\varphi}/L_{\varphi 0})^2$. $L_{\varphi}=(D\tau_{\varphi})^{0.5}$ is the phase-breaking length due to quasielastic Nyquist scattering, which is the main contribution to the phase breaking time in low-dimensional disordered systems.[20] τ_{φ} is the Nyquist dephasing time. $L_{\varphi_0}=(D\tau_{\varphi_0})^{0.5}$, where $1/\tau_{\varphi_0}(B)=1/\tau_{\varphi_0}(H=0)+1/\tau_H$, and $1/\tau_{\varphi_0}(H=0)$ is the inelastic electron-electron scattering rate. $1/\tau_H$ is the effective dephasing rate introduced by the magnetic field (H), and is given by $1/\tau_H=DW^2/12l_H^4$, and $l_H=(3\hbar^2/e^2AH^2)^{0.5}$ is the magnetic length with A the wire cross section. In order to perform a more reliable fit to Eq. (1), we have subtracted the contributions to the MR by the classical mechanism described by the three-band model ($\Delta R_{\mathrm{classical}}$). We have carried out a three-parameter fit (W, L_{φ}, and L_{φ_0}) to Eq. (1). The experimental and calculated resistances are in very good agreement for $H<12$ kOe as observed in Fig. 3(b). The values of the parameters inferred from the fit are $W\sim 40$ nm, $L_{\varphi}=52$ nm, and $L_{\varphi_0}=63$ nm at 10 K and $W\sim 40$ nm, $L_{\varphi}=53$ nm, and $L_{\varphi_0}=65$ nm at 5 K. We note that the value of the effective width obtained from the fit W is smaller than the physical width (100 nm). This difference could possibly be due to a reduction in the wire diameter caused by defect scattering by FIB irradiation, boundary scattering on some crystallographic defect or limitations in the description provided by the used model. Another feature to note is that the values of L_{φ} are comparable to, or slightly higher than, the estimated effective width of the wire, which suggests that the transport should be intermediate between the quasi-two-dimensional (2D) and quasi-1D regimes. Attempts to fit the MR using the theoretical forms for WAL in two and three dimensions have also been made giving a poor fit to the data. The NW could be considered as 1D system with respect to WAL.[7]

The relative intensity of the two effects (classical and WAL) could be altered by the wire dimensions and then WAL contribution can be tuned by reducing the wire diameter. An alternative way of enhancing the WAL contribution is the study of ultrathin Bi films with lateral size smaller than L_{φ} where the classical MR signal is expected to be reduced. Thus, WAL phenomena could be traced out to higher temperatures and higher magnetic fields, improving the resolution in the determination of the physical parameters derived from the analysis of the MR curves.

In summary, we have investigated the magnetotransport properties of individual single-crystalline Bi NWs 100 nm-diameter grown by electrodeposition. We achieved low-resistance Ohmic contacts to single Bi-NWs that were stable from 5 to 300 K by using FIB techniques. The MR showed evidence for WAL in 1D at temperatures below 10 K, with a phase breaking length of $\sim$100 nm.

This work was supported by Spanish Ministry of Science (through Project Nos. MAT2007-65965-C02-02 and MAT2008-06567-C02) including FEDER funding and the Aragon Regional Government. N. Marcano and S. Sangiao acknowledge financial support from Spanish CSIC (JAE-doc program) and Spanish MEC (FPU program).

[1] A. Boukai, K. Xu, and J. R. Heath, Adv. Mater. (Weinheim, Ger.) **18**, 864 (2006).
[2] J. Heremans, M. C. Thrush, Y. Lin, S. Cronin, Z. Zhang, M. S. Dresselhaus, and J. F. Mansfield, Phys. Rev. B **61**, 2921 (2000).
[3] Y. Lin, S. B. Cronin, J. Y. Ying, M. S. Dresselhaus, and J. Heremans, Appl. Phys. Lett. **76**, 3944 (2000).
[4] See, for example, J. J. Lin and J. P. Bird, J. Phys.: Condens. Matter **14**, R501 (2002).
[5] D. E. Beutler and N. Giordano, Phys. Rev. B **38**, 8 (1988).
[6] Z. Zhang, X. Sun, M. X. Dresselhaus, J. Y. Ying, and J. Heremans, Phys. Rev. B **61**, 4850 (2000).
[7] J. Heremans, C. M. Thrush, Z. Zhang, X. Sun, M. S. Dresselhaus, J. Y. Ying, and D. T. Morelli, Phys. Rev. B **58**, R10091 (1998).
[8] K. Liu, C. L. Chien, P. C. Searson, and K. Y. Zhang, Appl. Phys. Lett. **73**, 1436 (1998).
[9] O. Rabin, K. Nielsch, and M. S. Dresselhaus, Appl. Phys. A: Mater. Sci. Process. **82**, 471 (2006).
[10] S. B. Cronin, Y. Lin, O. Rabin, M. Black, J. Ying, M. Dresselhaus, P. Gai, J. Minet, and J. Issi, Nanotechnology **13**, 653 (2002).
[11] D. S. Choi, A. A. Balandin, M. S. Leung, G. W. Stupian, N. Presser, W. Chung, J. R. Heath, A. Khitun, and K. L. Lang, Appl. Phys. Lett. **89**, 141503 (2006).
[12] W. Shim, J. Ham, K. Lee, W. Y. Jeung, M. Johnson, and W. Lee, Nano Lett. **9**, 18 (2009).
[13] M. Plaza, M. Abuín, J. de la Venta, N. Marcano, S. Sangiao, L. Morellón, J. M. De Teresa, M. C. Sánchez, M. García, and L. Pérez (unpublished).
[14] I. Guillamón, H. Suderow, S. Vieira, A. Fernandez-Pacheco, J. Sesé, R. Cordoba, J. M. De Teresa, and M. R. Ibarra, New J. Phys. **10**, 093005 (2008).
[15] M. Barati and E. Sadeghi, Nanotechnology **12**, 277 (2001).
[16] N. W. Ashcroft and N. D. Mermin, *Solid State Physics* (Holt, Rinehart and Winston, New York, 1976), Chap. 12, p. 240.
[17] T. Hirahara, I. Matsuda, S. Yamazaki, N. Miyata, S. Hasegawa, and T. Nagao, Appl. Phys. Lett. **91**, 202106 (2007).
[18] A. Nikolaeva, D. Gitsu, L. Konopko, M. J. Graf, and T. E. Huber, Phys. Rev. B **77**, 075332 (2008).
[19] P. M. Echternach, M. E. Gershenson, H. M. Bozler, A. L. Bogdanov, and B. Nilsson, Phys. Rev. B **48**, 11516 (1993).
[20] B. L. Altshuler, A. G. Aronov, and D. E. Khmelnitskii, J. Phys. C **15**, 7367 (1982).